Sensors and Actuators A 314 (2020) 112230

Contents lists available at ScienceDirect

Sensors and Actuators A: Physical

journal homepage: www.elsevier.com/locate/sna

# High performance Cr doped ZnO by UV for $NH_3$ gas sensor

Puttipol Nakarungsee[a], Sasithorn Srirattanapibul[a], Chaisak Issro[b], I-Ming Tang[c], Sirikanjana Thongmee[a,*]

[a] Department of Physics, Faculty of Science, Kasetsart University, Bangkok, 10900, Thailand
[b] Department of Physics, Faculty of Science, Burapha University, Chonburi, 20131, Thailand
[c] Department of Mathematics, Faculty of Science, King Mongkut's University of Technology Thonburi, Bangkok, 10140, Thailand

ARTICLE INFO

*Article history:*
Received 27 April 2020
Received in revised form 17 July 2020
Accepted 24 July 2020
Available online 1 August 2020

*Keywords:*
Sensor
Cr-doped ZnO
Hydrothermal
UV illumination
Ammonia

ABSTRACT

In this work, Cr doped ZnO nanoparticles were synthesized by a hydrothermal method. Ammonia gas ($NH_3$) sensing was tested under UV illumination at room temperature. The irradiation returned the sensor after detecting the $NH_3$ molecules back to their initial states. More importantly, it created the electrons needed to ionize the oxygen molecules absorbed on the surface of the Cr:ZnO nanoparticles. This increase is necessary for the creation of more active surface sites which are necessary for the detection of the $NH_3$ molecular in air. It was found that the increase in the output of doped ZnO nanoparticles sensor is due both to the Cr doping and to the UV irradiation. For a $NH_3$ concentration of 50 ppm, the increase in the signal was 9 %. The results showed that the irradiated Cr doped ZnO nanoparticles have a higher sensitivity for detecting the presence of $NH_3$ gas at room temperature than the undoped and unirradiated ZnO nanoparticles.



## 1. Introduction

Nowadays, many researchers pay attention in gas sensors. This is because the gas sensors have various applications in fuel cells [1,2], in automobile industries (to detect the $NO_2$ from the vehicle exhaust) [3–6], in mining industries (for the detection of methane) [7], in fertilizer industries to detect the $NH_3$ [8–12] and in breathing analysis [11,13]. Therefore, to produce the high quality of gas sensors, low cost, low power consuming, highly sensitive, portability and small size gas sensor have to be considered [14]. For the small size gas sensor, many researchers try to develop the nanostructured materials to enhance gas sensing performance compared to bulk materials. This is because nanostructured materials have large surface area, small size, shape controllable, chemical composition and physiochemical stability [15].

In general, metal oxide (MO) can be used for the gas sensing application since they have possess excellent properties such as high sensing response, long term stability and easy to prepare [16]. When oxygen molecules are absorbed on these types of materials, the oxygen is ionized by capturing an electron for the conduction band of the MO, leading to the formation of surface depletion layer and to a higher resistance. There are different types of MO based gas sensors including $SnO_2$ [17], $TiO_2$ [18], ZnO [19,20], $WO_3$ [21] and $Fe_2O_3$ [22] with different morphologies. Among these MO, ZnO nanostructures have been extensively used as a gas sensors due to their excellent sensing response, good selectivity, low cost, easy preparation, good thermal and chemical stability and non-toxicity. Moreover, ZnO is intrinsic n-type semiconductor with wide band gap of 3.37 eV and a large exciton binding energy of 60 meV [23,24]. For ZnO, the difference in the energies of the valence band and conduction band are large and relatively high temperatures (300–500 °C) are needed to excite the valence band electrons. Traditional gas sensor based on ZnO must operate at these temperatures. Zhu and Zeng [25] reported that gas sensors with high sensing properties, simultaneously operating at room temperature are considerably more attractive owing to their low power consumption, high security and long-term stability. ZnO as semiconducting metal oxide is considered as the promising resistive-type gas sensing material, but elevated operating temperature becomes the bottleneck of its extensive applications in the field of real-time gas monitoring, especially in flammable and explosive gas atmosphere. Moreover, Srirattanapibul et al. [26] revealed that the photoelectron generating efficiency of ZnO can be enhanced by decorating them on reduced graphene oxide (rGO) or doping ZnO with impurity ions of another valance. The appropriate doping will provide the electronic defects which helps to increase the influence of oxygen partial pressure on the conductivity. Normally, there are two directions for improving the performance of ZnO-based gas sensors: one is doping

* Corresponding author.
*E-mail address:* fscisjn@ku.ac.th (S. Thongmee).

https://doi.org/10.1016/j.sna.2020.112230
0924-4247/

with metal elements [27–29] or heavy metal [30,31] and another one is fabricating sensors by using one or several nanostructures as gas sensing elements [32–34].

There are several ways to synthesis metal doping ZnO nanostructures such as spray pyrolysis [35], chemical vapor deposition [36], hydrothermal [5,31], thermal evaporation [37], sol–gel method [38] and template synthesis method [39]. Among these methods, hydrothermal method has been developed to synthesize a broad range of nanomaterials, including magnetic nanomaterials. The reaction parameters such as the type and concentration of the precursors, the solvent, the stabilizing agents and the reaction temperature and time, present important effects on the products.

In this work, chromium was used as the impurity to enhance the performance of the ZnO sensor. Using $Cr^{3+}$ ion doped ZnO, it can help to increase the efficiency of the photoelectron generation in ZnO. Since, the radius of $Cr^{3+}$ ion (0.062 nm) is nearly the same as that of $Zn^{2+}$ ion (0.072 nm). The $Cr^{3+}$ ion can replace with the $Zn^{2+}$ ion in the ZnO compound which introduce a large number of electrons in doping ZnO. The high performance gas sensor was achieved under UV light at room temperature. The sensing enhancement may be attributed to both the UV activation and Cr doping. The mechanism and the influence of doping elements on the sensing characteristics were also discussed.

## 2. Experimental details

### 2.1. Preparation of Cr-doped ZnO

The Cr-doped ZnO powders were prepared using hydrothermal method. Zinc nitrate hexahydrate [$Zn(NO_3)_2{\cdot}6H_2O$], chromium nitrate nonahydrate [$Cr(NO_3)_3{\cdot}9H_2O$] and sodium hydroxide (NaOH) were used as the precursors. The reagents were dissolved in deionized water at room temperature. Chromium solution was mixed with zinc solution in various molar ratios. Then, NaOH was added to maintain the pH value of zinc-chromium solution to 11. The resulting solutions were then transferred into a Teflon-lined autoclave. Then, the autoclave was heated at 180 C° for 20 h. When the autoclave cooled down to room temperature, the obtained white powder was washed several times with deionized water and dried in an oven at 110 C°. Finally, all the samples were characterized

The crystal structures of powdered samples were characterized on a Brucker D8-advanced, Karlsruhe, X-ray powder diffractometer (XRD) with CuKα radiation (λ = 1.5418 Å). Energy dispersive X-Ray Fluorescence (EDX) measurements were done to determine the actual amounts of chemical elements in each doped DMS specimen. The morphologies of all samples were examined using a scanning electron microscope (SEM) (FEI Quanta 450, Hillsboro, OR, USA). The ultraviolet absorption spectra (UV–vis) (Perkin Elmer, Lambda 650, Waltham, USA) were recorded for each sample to determine the shift in the value of the energy gap. The photoluminescence measurements were performed (iHR 550 spectrometer) using a 325 nm line from a He-Cd laser as the excitation source.

### 2.2. Sensor fabrication and measurement

5 mg of Cr-doped ZnO powder was mixed with 1 mL absolute ethanol and the mixture was sonicated for 30 min. Then, all mixtures were dropped on 1 cm × 1 cm Au-interdigitated electrodes at a temperature of 50 C°. The thickness of the film is about 50 μm. A two-way gas test chamber with a transparent window was used to perform the gas sensing measurement. UV-lamps (Toshiba FL20TBBL/18 W UV emission of wavelength 300–400 nm) were set up outside of the chamber next to the transparent window. The sensor was placed at the center of the testing chamber. $NH_3$ gas and air zero were mixed together in the tube before it was flowed into the testing chamber with the flow rate of 200 sccm. Then, the resistance of the sensor was measured until it is stable (no change in the resistance). The concentration of $NH_3$ was adjusted by $NH_3$ flow rate compare to air zero flow rate. The sensors were tested using 10–50 ppm of $NH_3$ under UV-illumination at room temperature with the humidity in range of 44–46 %. The gas response was tested with a digital multimeter (Fluke 289) which was connected to a personal computer to process the data. The gas sensing measurement system was shown in Fig. 1.

The response of the sensor is defined as

$$Sensor\ Response = \frac{R_a - R_g}{R_a} \times 100\%$$

where, $R_a$ is the resistance of the sensor in air and $R_g$ is the resistance of the sensor in the gas mixtures.

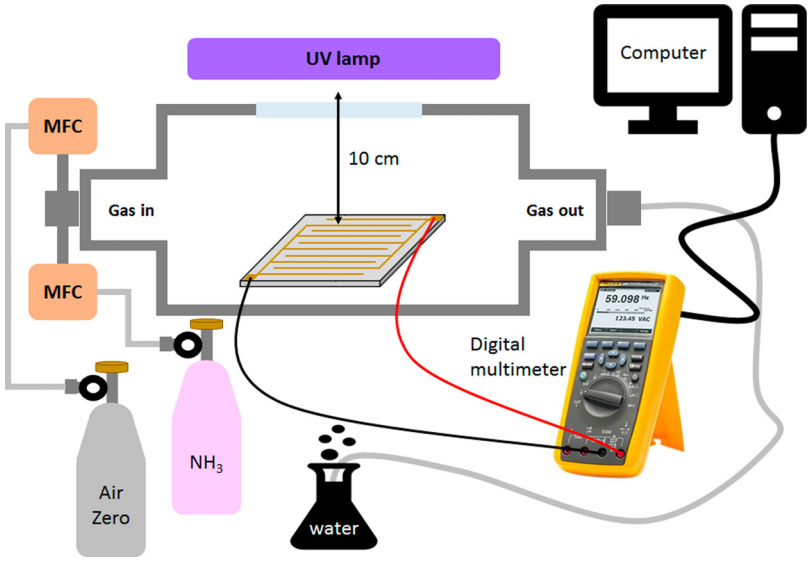


**Fig. 1.** Schematic diagram of gas sensing measurement system.

**Table 1**
Lattice constant and average crystallite size of various Cr-doped ZnO nanoparticles.

| Sample | a (Å) | c (Å) | Average crystallite size (nm) |
|---|---|---|---|
| Undoped ZnO | 3.2462 | 5.2065 | 20.3451 |
| 1 mol% Cr-doped ZnO | 3.2462 | 5.2030 | 21.7437 |
| 3 mol% Cr-doped ZnO | 3.2486 | 5.2030 | 21.7247 |
| 5 mol% Cr-doped ZnO | 3.2486 | 5.2030 | 19.3241 |

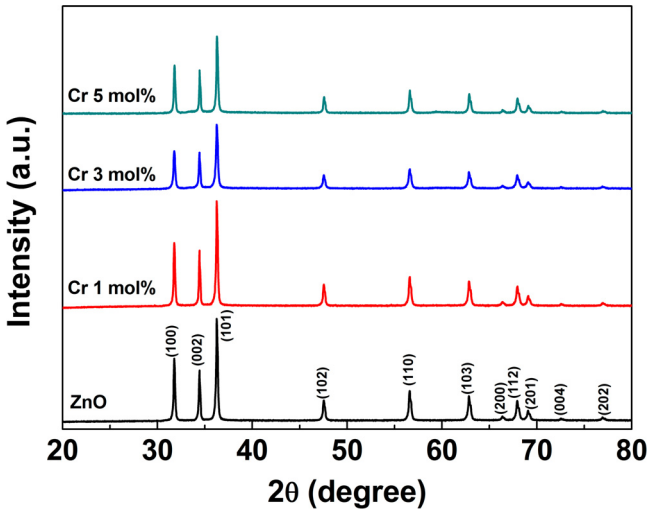


**Fig. 2.** XRD patterns of Cr-doped ZnO with different percentage of Cr.

**Table 2**
Energy dispersive X ray (EDX) data of undoped ZnO and Cr-doped ZnO nanoparticles.

| Sample | Zn (at%) | O (at%) | Cr (at%) |
|---|---|---|---|
| Undoped ZnO | 57.09 | 42.91 | – |
| 1 mol% Cr-doped ZnO | 58.23 | 42.50 | 0.48 |
| 3 mol% Cr-doped ZnO | 56.35 | 42.50 | 1.15 |
| 5 mol% Cr-doped ZnO | 55.52 | 42.23 | 2.25 |

## 3. Results and discussion

### 3.1. Characterization of properties

The crystal structure of ZnO and Cr-doped ZnO nanoparticles was characterized by XRD. The XRD patterns of ZnO and various Cr doped ZnO nanoparticles were shown in Fig. 2. The XRD patterns were taken using the CuK$\alpha$ line (wavelength 0.154 nm) at a scanning rate of 0.3°/s in the range of 2θ = 20–80°. All the samples exhibit the same diffraction peaks which were indexed to a hexagonal wurtzite ZnO structure (JCPDS 36–1451). There are no impurity peaks present in the patterns and no Cr peak was appeared.

Having the refection angles and the Miller indices for each peak in the XRD patterns, the lattice parameters **a**, **c** and average crystallite size can easily be determined. The values of the lattice parameters and average crystallite size for the different Cr-doped ZnO nanoparticles are listed in Table 1. Since, the radius of $Cr^{3+}$ ion (0.062 nm) is nearly identical to the ZnO structure. If the Cr substituted into the ZnO nanoparticles and given that radius of the $Cr^{3+}$ ion in an octahedron interstitial in ZnO is 0.061 nm and the radius $Zn^{2+}$ ion is 0.072 nm, there would be no changes in the values of the lattice parameters [40]. If the $Cr^{3+}$ ion replaced either the $Zn^{2+}$ ion in the ZnO compound or went into the interstitial positions in wurtzite structure as is seen in Table 1.

EDX measurements were used to confirm the existing of Cr and the other elements in the samples. The results are shown in the Table 2. From the result, one can see that the atomic percentage (at%) of Cr increases as the increasing of Cr doping.

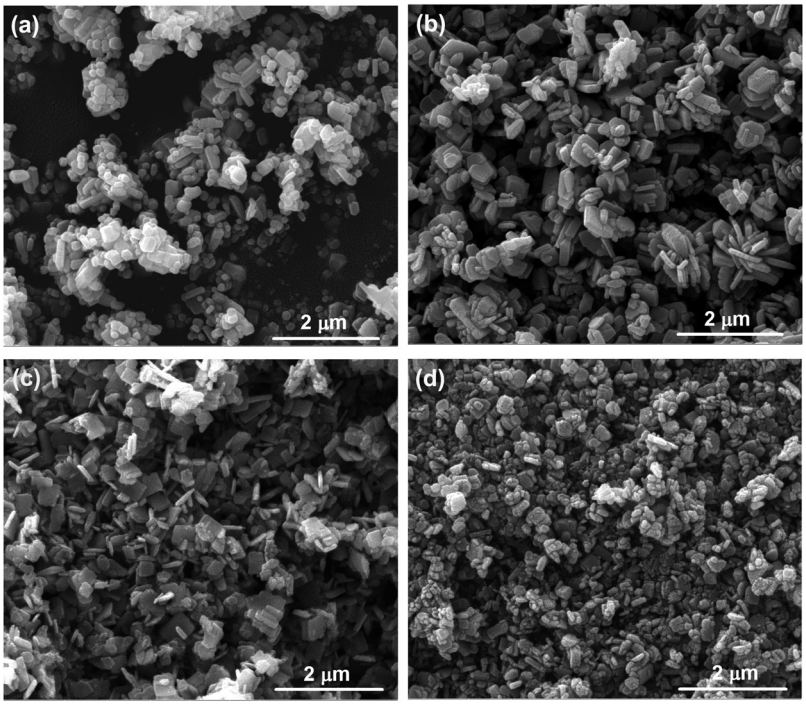


**Fig. 3.** SEM images of ZnO nanoparticles with different mol% of Cr-doped ZnO: (a) undoped ZnO, (b) 1 mol% Cr, (c) 3 mol% Cr and (d) 5 mol% Cr samples.

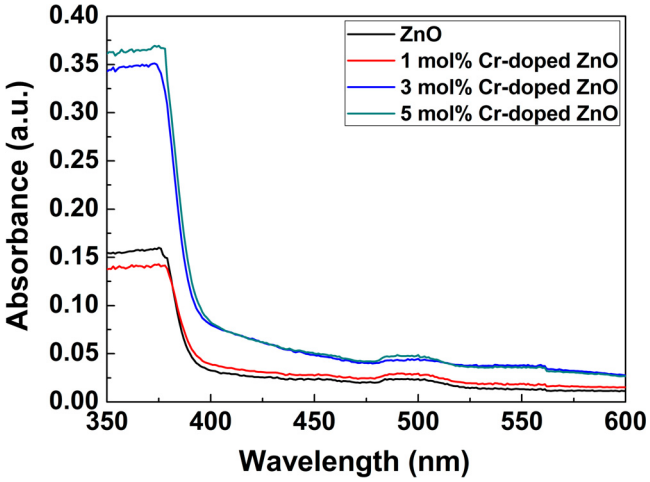


**Fig. 4.** UV–vis absorption spectra of various Cr-doped ZnO nanoparticles.

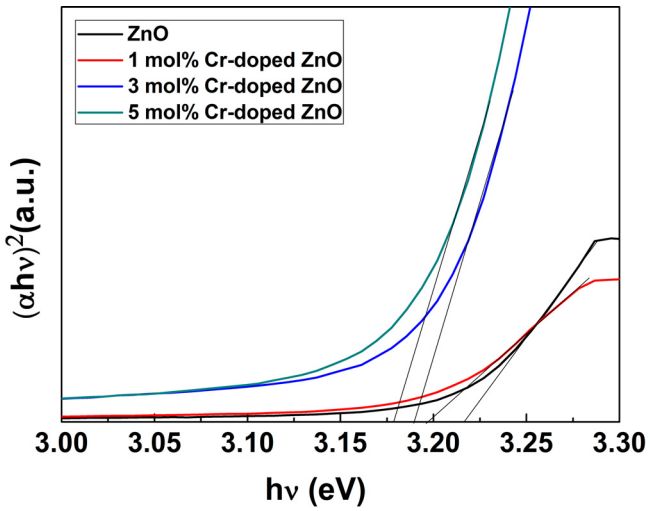


**Fig. 5.** Optical band gap of various Cr-doped ZnO nanoparticles.

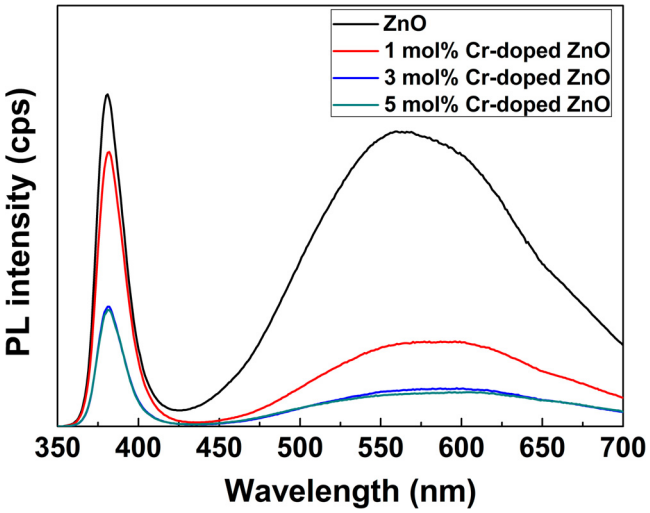


**Fig. 6.** PL spectra of ZnO and all Cr-doped ZnO nanoparticles.

The morphology of ZnO and Cr-doped ZnO nanoparticles was investigated by SEM. Fig. 3 shows SEM images of ZnO nanoparticles and Cr-doped ZnO nanoparticles with different amount of Cr doping. Fig. 3(a) is undoped ZnO nanoparticles. It is seen to be block-shape. Fig. 3(b) is the SEM image of 1 mol % Cr-doped ZnO sample. The result shows that the particles change to thick flake-shape. When the Cr is increased to 3 mol%, the structure of the particles is similar to the 1 mol% Cr-doped ZnO sample but the particles change to be thin flake- shape with small nanorods. This can be seen in Fig. 3(c). Moreover, SEM image of Fig. 3(d) shows that the structure of 5 mol% Cr-doped ZnO is similar to the 1 mol% Cr-doped ZnO sample but the particle size is decreased with the increasing of Cr doping. The 5 mol% Cr-doped ZnO sample shows the roughness on the particles surface. This might be the result of the excess Cr-dopant agglomeration [41].

The optical property of ZnO and Cr-doped ZnO nanoparticles is determined by UV–vis spectrometer. Fig. 4 shows the UV–vis absorption spectra of various Cr doped ZnO nanoparticles. The energy needs to excite electron from the valence band to the conduction band that relates to the incident light wavelength ($E = hc/\lambda$). If the wavelength is not short enough, there are only few electrons in the conduction band [42] and the reaction between gas and sensor is very lows. The absorption increased for higher Cr molar ratio. A sharp absorption band edge around 376 nm is in the UV range and shift to the higher wavelength side with the Cr concentration. This significant red shift occurs. It might be due to the spin-correlated exciton formation or to the crystal deformation through doping [43].

The data from Fig. 4 can be used to re-plot as $(\alpha h\upsilon)^2$ vs $h\upsilon$. The value of the optical band gap can be obtained by extrapolating the liner part of the Tauc relation $(\alpha h\nu)^2 = h\nu - E_g$, where $\alpha$ is absorption coefficient, $h$ is Planck's constant, $\nu$ is photon frequency and $E_g$ is optical band gap [44]. The plots are shown in Fig. 5.

The estimated band gap energies of the resulting samples are about 3.22, 3.20, 3.19 and 3.18 eV for undoped ZnO, 1 mol%, 3 mol% and 5 mol% Cr-doped ZnO, respectively. It can be seen that the increasing of Cr molar ratio made the absorption edges of the sensitized materials red-shifted.

Fig. 6 shows the PL spectra of the Cr-doped ZnO with different molar proportions. There are two peaks in the PL spectra of each sample. The first peak is in the range of 378–380 nm. These peaks are the near band edge (NBE) peak and are known as the exciton peaks. They are the emissions when the $(e^-/h^+)$ pair created. When an electron which is excited into the conduction band leaving behind a hole $(h^+)$ in the valance band interacts with the hole is self-annihilated and releases the energy difference between the highest occupied molecular orbitals (HUMO) energy states in the valence band and the lowest unoccupied molecular orbitals (LOMO) energy states in the valence band minus the binding energy of the exciton. The broad band in the range between 400–700 nm are due transmission to defect states created during the fabrication of the nanoparticles or to impurities doped into the ZnO nanoparticles. The intensities of the sub-spectra in the broad peak indicates the presence of the defects causing the particular component of the PL spectra. The portions of the PL spectra between 430–490 nm are due to the presence of Zn vacancies and Zn interstitials. While the spectra between 490–700 nm is due to the presence of O vacancies and O interstitials [45].

### 3.2. Results of sensing tests

The results of the sensing measurements and discussion of them are done using Figs. 7,8,9,10,11. Fig. 7 shows the sensor response of the undoped ZnO nanoparticles with and without UV irradiation when exposed to $NH_3$ concentration of 50 ppm of $NH_3$ at room temperature.

With UV activation, the sensitivity of undoped ZnO nanoparticles is much higher than that without UV exposure and the response time is shorter than without UV activation. The undoped ZnO nanoparticles under the UV illumination shows a maximum

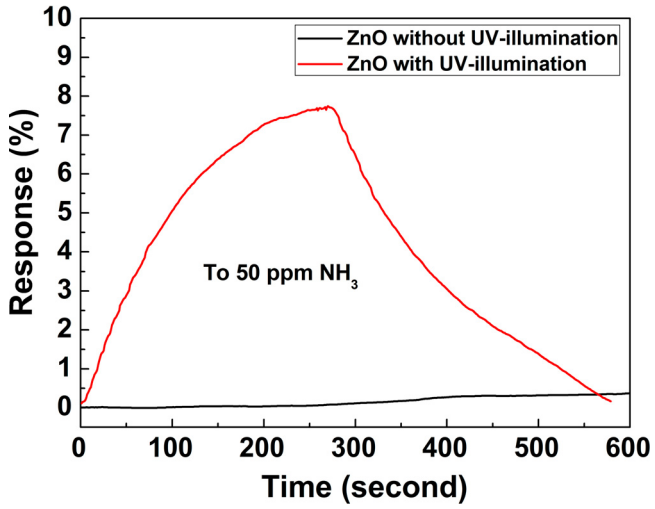


**Fig. 7.** Sensor response of undoped ZnO with and without UV-illumination under 50 ppm of $NH_3$ at room temperature.

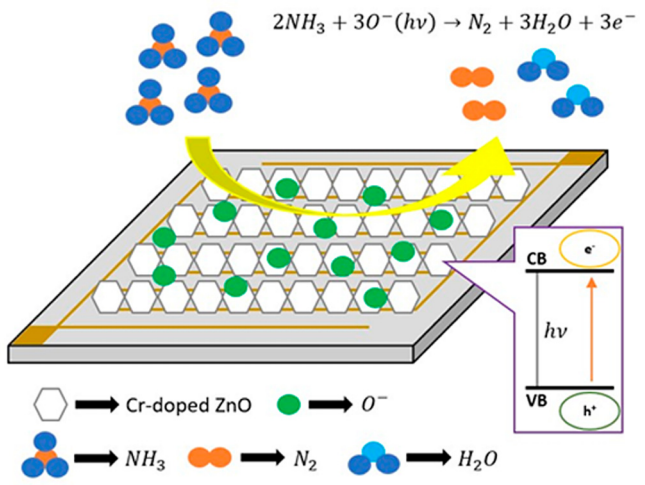


**Fig. 8.** Schematic of the surface of a Cr-doped ZnO sensors. The white hexagonal represent the individual ZnO nanoparticles.

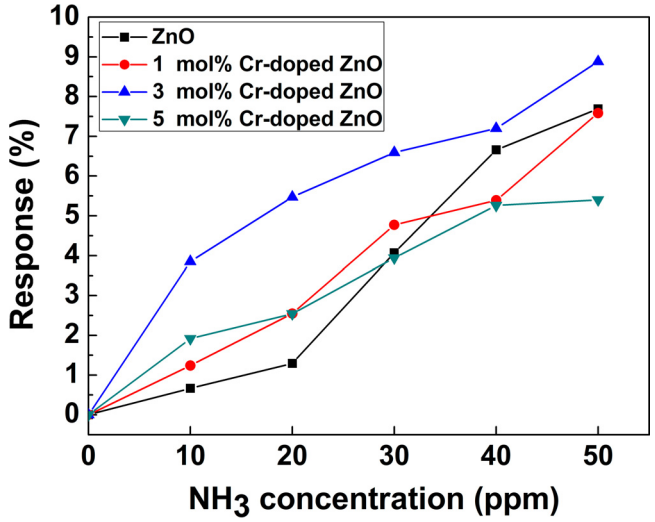


**Fig. 9.** Maximum sensor response of all Cr-doped ZnO nanoparticles with UV-illumination under various $NH_3$ concentration at room temperature.

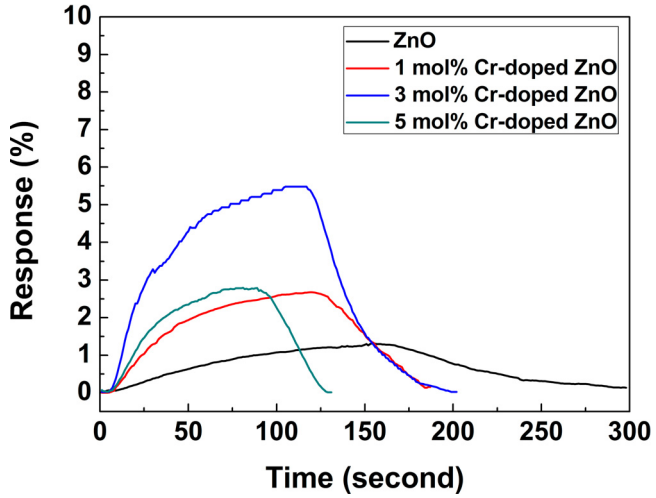


**Fig. 10.** Sensor response of all Cr-doped ZnO nanoparticles with UV-illumination under 20 ppm of $NH_3$ at room temperature.

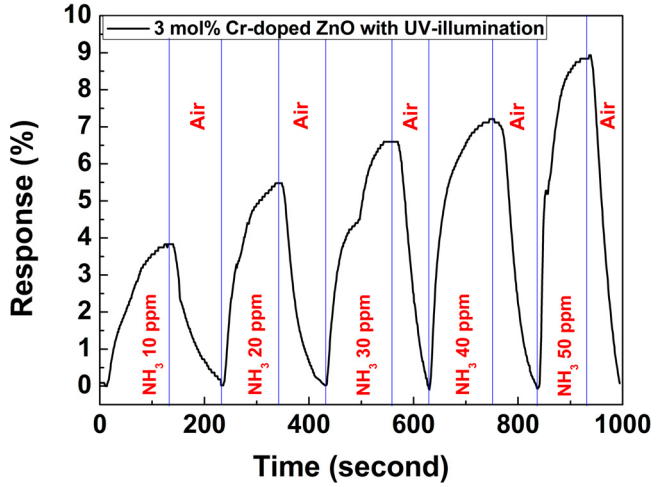


**Fig. 11.** Response time and recovery time of 3 mol% Cr-doped ZnO nanoparticles with UV-illumination under various $NH_3$ concentration at room temperature.

response of 8.75 % after 270 s and then a complete recovery back to the initial state in 300 s.

The sensing mechanism can be explained as follows: when the UV light is on, the electron-hole pairs are created in ZnO nanoparticles. The electrons from the valence band are excited to the conduction band. Normally, for ZnO, the photo excited electrons and the hole left behind form into excitons which mean that the photoelectrons are not available for other tasks such as photocatalytic conversion in other chemical reactions that might take place at the surface. By adding other ions or using the ZnO to decorate reduced graphene oxide, this hindrance can be removed and the photocatalytic activity can be restored. In air ambient, the original adsorbed oxygen on the ZnO surface will interact with the conduction electrons being the photo excited electrons to produce$O^-$ $(h\nu)$. The chemical processes being described by the reaction equations:

$$O_2\,(g) \leftrightarrow O_2\,(ads)$$

$$h\nu + ZnO \leftrightarrow ZnO + h^+(h\nu) + e^-(h\nu)$$

$$O_2\ (ads) + e^-(h\nu) \longleftarrow O_2^-(h\nu)$$

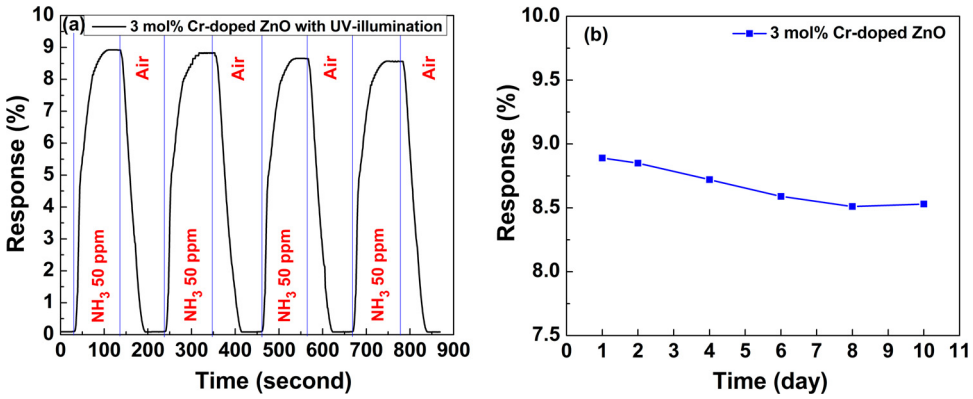


**Fig. 12.** Response of (a) Short-term stability and (b) long-term stability of 3 mol% Cr-doped ZnO nanoparticles with UV-illumination under 50 ppm concentration of $NH_3$ at room temperature.

$$O_2^-(h\nu) + e^-(h\nu) \longleftarrow 2O^-(h\nu)$$

The decrease in the number of electrons in the conduction band would lead to a rise in the resistance of the sensor ($R_a$) [37,46]. When the sensor is exposed to $NH_3$, gas molecules will react with the $O^-$ ($h\nu$) ions. This reaction is governed by:

$$2NH_3 + 3O^-(h\nu) \rightarrow N_2 + 3H_2O + 3e^- \text{Or } 2NH_3$$
$$+ 5O^-(h\nu) \rightarrow 2NO + 3H_2O + 5e^-$$

After this reaction, the electrons would then be released back to ZnO and made the resistance of the sensor decreased ($R_g$) [47]. Fig. 8 shows the schematics of the surface of a Cr-doped ZnO sensor which can operate at room temperature when the sensor is subject to UV irradiation.

The UV irradiation of the doped and undoped ZnO nanoparticles causes the electrons in the valence band to be photo excited to the conduction band where the electrons ($e^-$) and the holes ($h^+$) left behind to form the excitons which hinders the photocatalytic activity. The $Cr^{3+}$ ions restore some of the activity and created active surface sites where $O^-$ ions can be created. These $O^-$ can interact with the $NH_3$ molecules releasing the electron back to the conduction band, causing a drop in the resistance of the sensor.

Fig. 9 shows the response of sensors as a function of $NH_3$ concentration. It can be seen that all the Cr-doped ZnO based sensors have higher response than the undoped ZnO based sensor until the concentration reached 30 ppm of $NH_3$. A reason of this phenomenon of the resistance of Cr-doped ZnO nanoparticles becoming lower than that of the undoped ZnO is that $Cr^{3+}$ ion is initially replacing the $Zn^{2+}$ ion. For higher doping levels, the $Cr^{3+}$ ion may not be substituting into the $Zn^{2+}$ sites. It may be going into the interstitial sizes inside the ZnO or on the surface. Evidence of the latter is seen in the SEM image of the 5 mol % Cr-doped ZnO nanoparticles. Therefore, we observed a roughness in the surface of the nanoparticles which may due to the agglomeration of the excess Cr dopant on the surface. The response of this level of Cr doping would be different from the response at lower levels. At lower levels, additional active surface sites would be created because of the substitution. This would not be true if the excess $Cr^{3+}$ ion did not replace the $Zn^{2+}$ ion. The 3 mol% Cr-doped ZnO shows the highest sensor response to $NH_3$. It reached to 9% when exposed to 50 ppm of $NH_3$.

Fig. 10 shows the response time and the recovery time of the various Cr-doped ZnO nanoparticles exposed to 20 ppm of $NH_3$ subjected to UV irradiation at room temperature. It reveals that the Cr-doped ZnO sensors have good response time and recovery time which are shorter than that of the undoped ZnO sensors. The undoped ZnO sensors have good response and recovery times of 160 s and 140 s, respectively. When the Cr dopant is increased, the response time and the recovery time decreased. The quick response time and recovery time may be due to a faster oxidation and reduction of gas [48]. Also, the effect of Cr doping plays important to improve amount of donor electron [45] and adjusts energy level of ZnO [25]. From this hypothesis, we found from the literature reported before that the atomic content of Cr into ZnO structure can enhance the electrical conductivity of ZnO [41,49] and increase amount of defects [25]. This may cause and as consequence, the response and recovery time decrease. The 5 mol% Cr-doped ZnO needed the shortest time for maximum sensor response. The response and recovery time were 85 s and 40 s, respectively. However, the 3 mol % Cr-doped ZnO which needed 112 s to response and 88 s to recover had the best sensor response. All the sensors were able to recover to the baseline. These results show that all the sensor can be used several times.

Fig. 11 shows the response time and the recovery time of a 3 mol% Cr-doped ZnO nanoparticles exposed to 0–50 ppm of $NH_3$ under the UV illumination at room temperature. The result shows that the sensor respond increased with increasing $NH_3$ concentration. In addition, the sensing reaction increases sharply, when the concentration of $NH_3$ gas is given in high value while this sensor is able to recover to the baseline every time during the test.

The short-term stability measurement results of a 3 mol% Cr-doped ZnO nanoparticles sensor exposed to 50 ppm of $NH_3$ under the UV illumination at room temperature is shown in Fig. 12(a). The result show that the sensor is nearly constant respond and similar shapes in each cyclic measurement. Fig. 12(b) shows the results of long-term stability measurement in 10 days. From this result, the stability of the sensor was found to be good response at 3 mol% of Cr-doped ZnO nanoparticles. Although, in the beginning, it is slightly decreasing and then the response is quite constant. This is clearly to confirm that the sensor has a good stability and repeatable performance.

## 4. Conclusion

The undoped ZnO and Cr-doped ZnO nanoparticles were successfully synthesized by hydrothermal method. The XRD result showed that all the samples exhibit the same diffraction peaks which were indexed to a hexagonal wurtzite ZnO structure and no impurity peaks were presented in the patterns. SEM image of 5 mol% Cr-doped ZnO sample shows the roughness on the surface. This is caused by the agglomeration of the excess Cr dopants and the ones that were not used to replace the $Zn^{2+}$ ions in the wurtzite structure of ZnO. Moreover, Cr doping not only increases the UV–vis absorption but also decreased the energy band gap. For the sensing, the Cr doping increased the sensitivity and decreased

the response and recovery time. In this research, the 3 mol% Cr-doped ZnO showed the best performance as a sensing material.

## Author statement

The author statement is saying that none of the authors have financial interest in the results after the acknowledgement.

## Declaration of Competing Interest

The authors declare that there are no conflicts of interest regarding the publication of this paper.

## Acknowledgement

This work was supported by the funds from Department of Physics, Faculty of Science grant.

## References

[1] C.T. Holta, A.M. Azada, S.L. Swartza, R.R. Raob, P.K. Dutta, Carbon monoxide sensor for PEM fuel cell systems, Sens. Actuators B Chem. 87 (2002) 414–420.
[2] A. Modjtahedi, A. Amirfazli, S. Farhad, Low catalyst loaded ethanol gas fuel cell sensor, Sens. Actuators B Chem. 234 (2016) 70–79.
[3] D.J. Wales, J. Grand, V.P. Ting, R.D. Burke, K.J. Edler, C.R. Bowen, S. Mintova, A.D. Burrows, Gas sensing using porous materials for automotive applications, Chem. Soc. Rev. 44 (2015) 4290–4321.
[4] Y.J. Su, G.Z. Xie, H.L. Tai, S.D. Li, B. Yang, S. Wang, Q.P. Zhang, H.F. Du, H. Zhang, X.S. Du, Y. Jiang, Self-powered room temperature $NO_2$ detection driven by Triboelectric Nanogenerator under UV illumination, Nano Energy 47 (2018) 316–324.
[5] Y.J. Su, M.L. Yao, G.Z. Xie, H.P. Pan, H. Yuan, M. Yang, H.L. Tai, X.S. Du, Y. Jiang, Improving sensitivity of self-powered room temperature $NO_2$ sensor by triboelectric photoelectric coupling effect, Appl. Phys. Lett. 115 (2019), 073504.
[6] Y.J. Su, J.J. Wang, B. Wang, Tiannan Yang, B. Yang, G.Z. Xie, Y.H. Zhou, S.L. Zhang, H.L. Tai, Z.X. Cai, G. Chen, Y. Jiang, L.Q. Chen, J. Chen, Alveolus-inspired active membrane sensors for self-powered wearable chemical sensing and breath analysis, ACS Nano 14 (5) (2020) 6067–6075.
[7] P. Bhattacharyya, P.K. Basu, H. Saha, S. Basu, Fast response methane sensor using nanocrystalline zinc oxide thin films derived by Sol–Gel method, Sens. Actuators B Chem. 124 (2007) 62–67.
[8] R. Ghosh, A. Midya, S. Santra, S.K. Ray, Guha P.K, Chemically reduced graphene oxide for ammonia detection at room temperature, ACS Appl. Mater. Interfaces (2013) 7599–7603.
[9] H.Y. Li, C.S. Lee, D.H. Kim, J.H. Lee, Flexible room-temperature NH3 sensor for ultrasensitive, selective, and humidity-independent gas detection, ACS Appl. Mater. Interfaces 10 (2018) 27858–27867.
[10] C. Liu, H. Tai, P. Zhang, Z. Yuan, X. Du, G. Xie, Y. Jiang, A high-performance flexible gas sensor based on self-assembled PANI-$CeO_2$ nanocomposite thin film fortrace- level $NH_3$ detection at room temperature, Sens. Actuators B Chem. 261 (2018) 587–597.
[11] Y.J. Su, T.N. Yang, X. Zhao, Z.X. Cai, G. Chen, M.L. Yao, K. Chen, M. Bick, J.N. Wang, S.D. Li, G.Z. Xie, H.L. Tai, X.S. Du, Y. Jiang, J. Chen, A wireless energy transmission enabled wearable active acetone biosensor for noninvasive prediabetes diagnosis, Nano Energy 74 (2020), 104941.
[12] Y. Li, M. Jiao, H. Zhao, M. Yang, High performance gas sensors based on in-situ fabricated ZnO/polyaniline nanocomposite: the effect of morphology on the sensing properties, Sens. Actuators B Chem. 264 (2018) 285–295.
[13] H.L. Tai, S. Wang, Z.H. Duan, Y.D. Jiang, Evolution of breath analysis based on humidity and gas sensors: potential and challenges, Sens. Actuators B Chem. 318 (2020), 128104.
[14] A. Dey, Semiconductor metal oxide gas sensors: a review, Mat. Sci. Eng. B 229 (2018) 206–217.
[15] M.A. Gatoo, S. Naseem, M.Y. Arfat, A.M. Dar, K. Qasim, S. Zubair, Physicochemical properties of nanomaterials: implication in associated toxic manifestations, Biomed Res. Int. 2014 (2014), 498420.
[16] B. Shouli, L. Dianqing, H. Dongmei, L. Ruixian, C. Aifan, C.C. Liu, Preparation, characterization of $WO_3$–$SnO_2$ nanocomposites and their sensing properties for $NO_2$, Sens. Actuators B Chem. 150 (2010) 749–755.
[17] L. Li, S. He, M. Liu, M. Zhang, W. Chen, Three-dimensional mesoporous graphene aerogel-supported $SnO_2$ nanocrystals for high-performance $NO_2$ gas sensing at low temperature, Anal. Chem. 87 (2015) 1638–1645.
[18] T. Xie, N. Sullivan, K. Steffens, B. Wen, G. Liu, R. Debnath, A. Davydov, R. Gomez, A. Motayed, UV-assisted room-temperature chemiresistive NO2 sensor based on $TiO_2$ thin film, J. Alloys Compd. 653 (2015) 255–259.
[19] Q. Zhang, G. Xie, M. Xu, Y. Su, H. Tai, H. Du, Y. Jiang, Visible light-assisted room temperature gas sensing with ZnO-Ag heterostructure nanoparticles, Sens. Actuators B Chem. 259 (2018) 269–281.
[20] S. Wang, H.L. Tai, B.H. Liu, Z.H. Duan, Z. Yuan, H. Pan, Y.J. Su, G.Z. Xie, X.S. Du, Y.D. Jiang, A facile respiration-driven triboelectric nanogenerator for multifunctional respiratory monitoring, Nano Energy 58 (2019) 312–321.
[21] B.U. Wojcik, T.A. Vincent, M.F. Chowdhury, J.W. Gardner, Ultrasensitive $WO_3$ gas sensors for $NO_2$ detection in air and low oxygen environment, Sens. Actuator B: Chem. 181 (2013) 735–742.
[22] P. Sun, W. Wang, Y. Liu, Y. Sun, J. Ma, G. Lu, Hydrothermal synthesis of 3D urchin- like A-$Fe_2O_3$ nanostructure for gas sensor, Sens. Actuators B Chem. 173 (2012) 52–57.
[23] P. Rai, Y.S. Kim, H.M. Song, M.K. Song, Y.T. Yu, The role of gold catalyst on the sensing behavior of ZnO nanorods for CO and $NO_2$ gases, Sens. Actuators B Chem. 165 (2012) 133–142.
[24] Q. Wan, Q.H. Li, Y.J. Chen, Fabrication and ethanol sensing characteristics of ZnO nanowire gas sensors, Appl. Phys. Lett. 84 (18) (2004) 3654–3656.
[25] L. Zhu, W. Zeng, Room-temperature gas sensing of ZnO-based gas sensor: a reviewSens, Actuators A: Physical. 267 (2017) 242–261.
[26] S. Srirattanapibul, I.M. Tang, S. Thongmee, Photo catalytic reduction of $Cr^{6+}$ by ZnO decorated on reduced graphene oxide (rGO) nanocomposites, Mater. Res. Bull. 122 (2020), 110705.
[27] A. Yu, J. Qian, H. Pan, et al., Micro-lotus constructed by Fe-doped ZnO hierarchically porous nanosheets: preparation, characterization and gas sensing property, Sens. Actuators B Chem. 158 (1) (2011) 9–16.
[28] K. Zheng, L. Gu, D. Sun, X. Mo, G. Chen, The properties of ethanol gas sensor based on Ti doped ZnO nanotetrapods, Mater. Sci. and Engin. B: Solid-State Mater. Adv.Technol. 166 (1) (2010) 104–107.
[29] N. Han, X. Wu, D. Zhang, G. Shen, H. Liu, Y. Chen, CdO activated Sn-doped ZnO for highly sensitive, selective and stable formaldehyde sensor, Sens. Actuators B Chem. 152 (2) (2011) 324–329.
[30] Q. Xiang, G. Meng, Y. Zhang, et al., "Ag nanoparticle embedded- ZnO nanorods synthesized via a photochemical method and its gas-sensing properties,", Sens. Actuators B Chem. 143 (2) (2010) 635–640.
[31] S. Wang, Y.D. Jiang, H.L. Tai, B.H. Liu, Z.H. Duan, Z. Yuan, H. Pan, G.Z. Xie, X.S. Du, Y.J. Su, An integrated flexible self-powered wearable respiration sensor, Nano Energy 63 (2019), 103829.
[32] H.L. Taia, Z.H. Duana, Z.H. Hea, X. Lib, J.L. Xuc, B.H. Liua, Y.D. Jianga, Enhanced ammonia response of $Ti_3C_2T_x$ nanosheets supported by $TiO_2$ nanoparticles at room temperature, Sens. Actuators B Chem. 298 (2019), 126874.
[33] Y.J. Su, G.Z. Xie, S. Wang, H.L. Tai, Q.P. Zhang, H.F. Du, H.L. Zhang, X.S. Du, Y.D. Jiang, Novel high-performance self-powered humidity detection enabled by triboelectric effect, Sens. Actuators B Chem. 251 (2017) 144–152.
[34] T.M. Li, W. Zeng, Z.C. Wang, Quasi-one-Dimensional metal-oxide-Based heterostructural gas-sensing materials: a review, Sens. Actuators B Chem. 221 (2015) 1570–1585.
[35] M. Rajendra Prasada, M. Harisa *, M. Sridharan, $NH_3$ sensing properties of surface modified Ce-doped nanostructuredZnO thin films prepared by spray pyrolysis method, Sens. Actuators A: Physical 269 (2018) 435–443.
[36] S. Ameen, M.S. Akhtar, M. Song, H.S. Shin, Vertically aligned ZnO nanorods on hot filament chemical vapor deposition grown graphene oxide thin film substrate: solar energy conversion, ACS Appl, Mater. Interfaces 4 (2012) 4405–4412.
[37] H.C. Ji, W. Zeng, Y.Q. Li, Gas sensing mechanisms of metal oxide semiconductors: a focus review, Nanoscale 11 (47) (2019) 22664.
[38] R. Sui, P. Charpentier, Synthesis of metal oxide nanostructures by direct Sol–Gel chemistry in supercritical fluids, Chem. Rev. 112 (2012) 3057–3082.
[39] Y. Boyjoo, M. Wang, V.K. Pareek, J. Liu, M. Jaroniec, Synthesis and applications of porous non-silica metal oxide submicrospheres, Chem. Soc. Rev. 45 (2016) 6013–6047.
[40] G. Srinet, R. Kumar, V. Sajal, Structural studies and band gap tuning of Cr doped ZnO nanoparticles, AIP Conf. Proc. 1591 (2014) 1476.
[41] C.H. Zhang, X.Y. Deng, P.Y. Wang, X.L. Wang, Y. Chen, H.I. Ma, D.J. Gengzang, Morphology controlled synthesis of Cr doped ZnO single-crystal nanorods for acetone gas sensor, Mater. Lett. 165 (2016) 83–86.
[42] A. Janotti, C.G. Van de Walle, Fundamentals of zinc oxide as a semiconductor, Rep. Prog. Phys. 72 (2009), 126501.
[43] T. Wu, Z. Wang, M. Tian, J. Miao, H. Zhang, J. Sun, UV excitation $NO_2$ sensor sensitized by ZnO quantum dots at room temperature, Sens. Actuator B: Chem. 259 (2018) 526–531.
[44] J. Tauc, Optical properties and electronic structure of amorphous Ge and Si, Mater. Res. Bull. 3 (1968) 37–46.
[45] A.B. Djurisic, W.C.H. Choy, V.A.L. Roy, Y.H. Leung, C.Y. Kwong, K.W. Cheah, G. Rao, W.K. Chan, H.F. Lui, C. Surya, Photoluminescence and Electron Paramagnetic resonance of ZnO tetrapod structures, Adv. Funct. Mater. 14 (9) (2004) 856–864.
[46] N.H. Al-Hardan, M.J. Abdullah, A.A. Aziz, Performance of Cr-doped ZnO for acetone sensing, Appl. Surf. Sci. 270 (2013) 480–485.
[47] T.Y. Chen, H.I. Chen, C.S. Hsu, C.C. Huang, J.S. Wu, P.C. Chou, W.C. Liu, Characteristic of ZnO nanorods-based ammonia gas sensors with a cross linked configuration, Sens. Actuator B: Chem. 221 (2015) 491–498.
[48] G.K. Hani, J.B.B. Rayappan, A highly selective room temperature ammonia sensor using spray deposited zinc oxide thin film, Sens. Actuator B: Chem. 183 (2013) 459–466.
[49] J. Qi, H. Zhang, S. Lu, X. Li, M. Xu, Y. Zhang, High performance indium-doped ZnO gas sensor, J. Nanomater. 2015 (2015) 1–6.

## Biographies

**Puttipol Nakarungsee** is a Ph.D. student in Department of Physics, Faculty of Science, Kasetsart University. He received his master degree from Kasetsart University. His research interests in area of zinc oxide for gas sensor applications.

**Sasithorn Srirattanapibul** is a Ph.D. student in Department of Physics, Faculty of Science, Kasetsart University. She received her master degree from Kasetsart University. Her research interests in area of graphene for gas sensor applications.

**Chaisak Issro** is an Assistant Professor in Department of Physics, Faculty of Science, Burapha University. He received his Dr.rer.nat degree from University of Vienna. His research interests in area of carbon nanotubes for gas sensor applications.

**I-Ming Tang** is a Professor in Department of Physics, Faculty of Science, Mahidol University. He received his Ph.D. from University of Cincinnati, USA. His research interests in area of Magnetic materials, Superconductor, Nanomaterials, Theoretical Condensed Matter Physics and Graphene for photocatalytic applications.

**Dr. Sirikanjana Thongmee** now is an Associate Professor of Physics; she was in Physics Department, Faculty of Science, Kasetsart University. Her research focus on the metal doped ZnO for spintronics and gas sensor applications, magnetic nanomaterials, Metal oxide decorated graphene oxide for Photocatalytic, sensing and 3D printing. Moreover, Dr. Sirikanjana Thongmee is also doing research on activated carbon from agricultural wasted for adsorbing the heavy metals, different type of poison gases and waste water.